

Control of transmission of right circularly polarized laser light in overdense plasma by applied magnetic field pulses

Guangjin Ma (马光金),¹ Wei Yu (余玮),¹ M. Y. Yu (郁明阳),^{2,3,*} Shixia Luan (栾仕霞),¹ and Dong Wu (吴栋)^{1,4}

¹State Key Laboratory of High Field Laser Physics, Shanghai Institute of Optics and Fine Mechanics, Chinese Academy of Sciences, Shanghai 201800, China

²Institute for Fusion Theory and Simulation and Department of Physics, Zhejiang University, Hangzhou 310027, China

³Institut für Theoretische Physik I, Ruhr-Universität Bochum, D-44780 Bochum, Germany

⁴Helmholtz Institute Jena, D-07743 Jena, Germany

(Received 17 February 2016; published 25 May 2016)

The effect of a transient magnetic field on right-hand circularly polarized (RHCP) laser light propagation in overcritical-density plasma is investigated. When the electron gyrofrequency is larger than the wave frequency, RHCP light can propagate along the external magnetic field in an overcritical density plasma without resonance or cutoff. However, when the magnetic field falls to below the cyclotron resonance point, the propagating laser pulse will be truncated and the local plasma electrons resonantly heated. Particle-in-cell simulation shows that when applied to a thin slab, the process can produce intense two-cycle light pulses as well as long-lasting self-magnetic fields.

DOI: [10.1103/PhysRevE.93.053209](https://doi.org/10.1103/PhysRevE.93.053209)

I. INTRODUCTION

Recently, it has been demonstrated by particle-in-cell (PIC) simulation that tunable circularly polarized terahertz (THz) radiation can be generated from the interaction of two-color left-hand circularly polarized laser light with strongly magnetized underdense plasma [1]. The frequency of electromagnetic waves (EMWs) in the optical regime is usually much higher than the electron gyrofrequency, with few exceptions [2,3]. Therefore, up to now, laser propagation in strongly magnetized plasmas in the $\Omega > \omega_L$ regime (where $\Omega = eB/mc$ and ω_L are the gyro and EMW frequencies, $-e$ and m are the charge and mass of the electron, and c is the light speed in vacuum) has not gained much attention. This is because although giga- and even teragauss magnetic fields exist in and around cosmic objects such as pulsars, black holes, and magnetars [4–6], in the laboratory magnetic fields only up to the megagauss level have been produced using traditional methods such as by strong implosion and/or shock-wave driven compression [7], powerful multicoil magnets [8], etc. On the other hand, in high-intensity short-pulse laser interaction with solid targets, highly time- and space-localized extremely intense magnetic fields can be self-generated by the baroclinic effect [9], electron temperature anisotropy [10], relativistic electron beams [11], etc., and the topic has been widely investigated [12–15]. In fact, self-generation of magnetic fields at the gigagauss level have been reported in experiments [16] and numerical simulations [17]. In view of the ongoing worldwide effort to further advance even shorter-pulse higher-intensity lasers and stronger pulsed magnetic fields [15,18], one can expect that highly space-time-localized hundreds of megagauss functional magnetic fields should be available in the near future from advanced laser-target interaction designs. The possibility of penetration of intense laser light into overdense plasma can have many applications, especially for diagnostics of material structures and in the fast ignition

scheme of inertial confinement fusion. It is therefore of interest to look into the behavior of laser-plasma interaction involving such high magnetic fields, especially in the $\Omega > \omega_L$ regime.

The optical properties of a linear medium are governed by its refractive index $N \equiv ck_L/\omega_L = \varepsilon^{1/2}$ [19], where $k_L = 2\pi/\lambda_L$, ω_L , and c are the EMW wave vector, frequency, and vacuum speed, and ε is the dielectric constant of the medium. For unmagnetized plasma, one has $\varepsilon = 1 - \omega_p^2/\omega_L^2$ [20], where $\omega_p = (4\pi n_0 e^2/m)^{1/2}$ is the plasma frequency. Thus, EMWs cannot penetrate an overdense plasma, where $\omega_p > \omega_L$. However, for right-hand circularly polarized (RHCP) EMWs propagating along an applied magnetic field, the dielectric constant is $\varepsilon_B = 1 - (\omega_p^2/\omega_L^2)(1 - \Omega/\omega_L)^{-1}$. Thus, $\varepsilon_B > 1$ for a plasma with $\Omega/\omega_L > 1$, so that a sufficiently magnetized overdense plasma slab can be transparent. For convenience, in the following we normalize the plasma density by the critical density $n_c = m\omega_L^2/4\pi e^2$ and the applied magnetic field by $m c \omega_L / e$, so that one obtains the simple forms $\varepsilon = 1 - n_0$ and $\varepsilon_B = 1 - n_0/(1 - B_0)$ for RHCP EMW propagation in unmagnetized and magnetized plasmas, respectively. We note that for left-hand circularly polarized EMWs, the minus sign in the denominator is replaced by a plus sign, so that the wave cannot propagate in a solid-density plasma for any magnetic field strength [1,20].

As an example, we consider RHCP EMW propagation at normal incidence along the applied magnetic field through an overdense plasma slab with $n_0 = 100$ and $B_0 = 3$ (corresponding to $B_0 \sim 320$ megagauss in dimensional units for $\lambda_L = 1 \mu\text{m}$ light). According to the linear theory, we have the refractive index $N = \sqrt{\varepsilon_B} \sim 7.141$. Thus, from the Fresnel formula, the transmission coefficient for propagation from vacuum to plasma is $\mathcal{T}_{\text{in}} = 2/(1 + N) \sim 0.246$ and from plasma to vacuum $\mathcal{T}_{\text{out}} = 2N/(1 + N) = 1.754$. Accordingly, the transmission coefficient of the plasma slab is $\mathcal{T} = \mathcal{T}_{\text{in}}\mathcal{T}_{\text{out}} = 0.431$, so that about 43% of the incident RHCP EMW wave field (about 19% of the wave energy) can be transmitted. In this paper, we verify by particle-in-cell (PIC) simulation this property for nonlinear RHCP EMWs, and we show that it could be invoked to produce intense few-cycle

*myyu@zju.edu.cn

light pulses by allowing only a part of an intense laser pulse to pass through the plasma slab. The evolution of the process is investigated in detail, and it is found that a long-living quasistatic lateral magnetic field is generated in the plasma. Although relatively weak few-cycle light pulses have been successfully realized and applied for some time in connection with diagnostics and manipulation of ultrafast phenomena [21], intense short-pulse laser light useful for generation of ultrashort pulse or wavelength radiation, charged-particle acceleration, medical cell repair, tumor treatment, etc., is still being widely investigated [22–28].

II. PIC SIMULATION PARAMETERS

The length of the PIC simulation box is $5\lambda_L$, where λ_L is the laser central wavelength. The box contains 1000 cells, or 200 cells per λ_L . A thin uniform plasma target of density $n_0 = 100n_c$ is located in $2\lambda_L \leq x \leq 2.055\lambda_L$, occupying 11 cells each containing 1000 macro electrons and ions. The ion charge number is $Z = 1$ and the ion-to-electron mass ratio is $m_i/m_e = 1836$. In the simulation, both the electrons and ions are mobile and have zero initial temperature. Thus, any modification of the slab by the laser and/or the applied magnetic field should be observable. Note also that since the few-cycle pulse is created right at the beginning of the interaction, the scheme can still be operative even if the target is destroyed by the interaction.

The applied magnetic field is assumed to be a spatially uniform transient pulse, covering the entire simulation box, even though it is only needed inside the thin target (since it has no effect in the vacuum regions). Depending on the required property of the transmitted pulse, in practice only a field that decreases from $B_0 > 1$ to $B_0 < 1$ sufficiently fast and covering a region defined by the laser spot and target thickness is needed. Accordingly, we model the applied magnetic field by a step function bounded by sinusoidal rise and fall fronts, namely $\mathbf{B}_0 = \hat{x} B_0 \{g[(t - t_1)/\tau_1] \sin[\pi(t - t_1)/2\tau_1] + g[(t - t_1 - \tau_1)/\tau_2] + g[(t - t_1 - \tau_1 - \tau_2)/\tau_1] \cos[\pi(t - t_3)/2\tau_3]\}$, where B_0 is the normalized field strength, and $g[(t - t_1)/\tau_1]$ is the step function: $g = 1$ for $t_1 < t < t_1 + \tau_1$ and $g = 0$ elsewhere. The time scales $\tau_{1,2,3}$ are of the order of the light wave period.

A RHCP laser pulse propagates in the positive x direction from the left boundary (at $x = 0$) of the simulation box. The laser electric field is given by $\mathbf{E}(0, t) = a(0, t) \exp(2i\pi t/T_L + \pi/2) \hat{\mathbf{e}}_R + c.c.$, where $a(0, t) = a_0 \sin^2(\pi t/\tau)$ is the pulse envelope, a_0 is the laser parameter, or the peak wave electric field normalized by $m_e c \omega_L / e$, $\hat{\mathbf{e}}_R = \hat{y} + i\hat{z}$, \hat{y} , and \hat{z} are unit vectors in the y and z directions, respectively, and τ is the pulse duration normalized by T_L .

For the 1D 3V (one-dimensional in space and three dimensional in velocity) collisionless PIC simulations, we set $a_0 = 0.1$, $\tau = 20T_L$, $B_0 = 3$, $\tau_1 = 1T_L$, $\tau_2 = 1.5T_L$, $\tau_3 = 1T_L$, and $n_0 = 100n_c$. As in the linear theory discussed above, the initial plasma is assumed to be cold. The laser-plasma interaction is thus not highly nonlinear [29], and the slab is not destroyed, so that comparison of the simulation results with that from the theory can be made. The magnetic pulse strength and duration are also such that the plasma is not destroyed before the desired light transmission is complete, as would happen if the electron cyclotron frequency is too close

to the laser frequency because of cyclotron resonance and rapid electron heating. Higher-intensity lasers can also be used in order to enhance (e.g., by self-focusing and transparency) the resulting short light pulse, as long as the target is not significantly modified in the time of interest. Although no optimization has been made, the timing of the magnetic pulse in the simulation is such that its peak value roughly overlaps a high intensity front part of the incident laser pulse, so that a short but intense portion of the latter is transmitted.

III. SIMULATION RESULTS

Figure 1 shows how the RHCP laser pulse interacts with the transiently magnetized plasma target. The black dashed lines mark the on and off times of the magnetic field $B_0(t)\hat{x}$. The evolution can be seen in panels (a) and (b) for the projections E_y and B_z of the wave (and the much weaker self-consistent/-generated) electric and magnetic fields in the y and z directions, respectively. Recall that the incident, transmitting, and transmitted pulses are circularly polarized. For clarity, in (c) and (d) we show the space-time dependence of the magnitudes of the total (except \mathbf{B}_0) electric and magnetic fields $|E| = [E_y(t)^2 + E_z(t)^2]^{1/2}$ and $|B| = [B_y(t)^2 + B_z(t)^2]^{1/2}$, respectively. The laser pulse propagates in the left vacuum region at the light speed c . Its leading front arriving at the still-unmagnetized overdense target plasma is reflected and forms a standing-wave pattern with the still incoming light. The external magnetic pulse is applied and appears at $t = 8T_L$, and when $B_0 > 1$ occurs at $t \sim 8.4T_L$, the

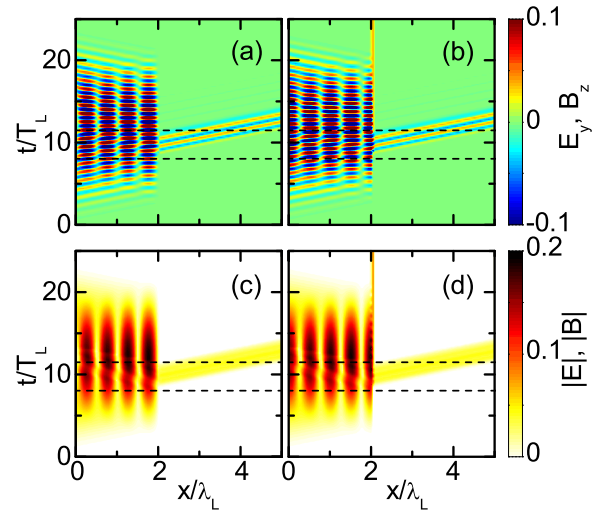


FIG. 1. (a) Evolution of the component E_y of the (incident, reflected, and transmitted) RHCP wave electric fields. Interference between the incident and reflected waves can be clearly seen in the front vacuum region. The black dashed lines mark the turning-on and -off times (including the ramps) of the applied magnetic field. (b) The z component of the wave and self-generated magnetic fields. (c) The magnitude $|E|$ of the wave electric fields. (d) The magnitude $|B|$ of the wave and self-generated magnetic fields. Note that the self-generated field exists only inside the target, appearing as a thin red region (line) in $2\lambda_L \leq x \leq 2.055\lambda_L$, and it persists even after the laser-plasma interaction has ended. The laser parameters are $a_0 = 0.1$ and $\tau = 20$.

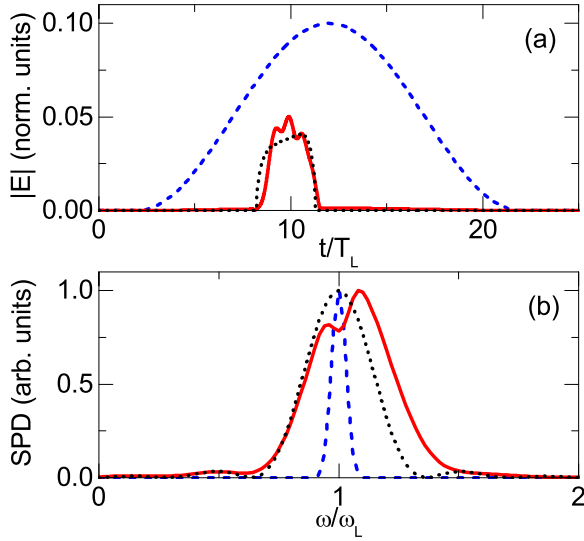


FIG. 2. (a) Evolution of the amplitudes of the incident (blue dashed curve) and transmitted (red solid curve) RHCP pulses. The maximum transmitted light wave electric field $|E| \sim 0.05$ appearing at $t \sim 10$ corresponds to the light intensity $I \sim 5 \times 10^{15} \text{ W cm}^{-2}$. (b) The corresponding spectra. The black dotted curves for the transmitted pulse are obtained from the Fresnel formula. The spectra curves have been normalized by their own maxima. The laser and plasma parameters are the same as in Fig. 1.

slab becomes transparent. A short but high-intensity portion of the laser pulse can pass through the slab before the applied magnetic pulse vanishes at $t \sim 11.50T_L$. The slab then again becomes opaque, cutting off the remaining part of the laser pulse, (see also the discussion at the end of this section). The full width at half-maximum (FWHM) and intensity of the transmitted ultrashort light pulse are $\tau_{tr} \sim 1.785T_L$ and $a_{tr} \sim 0.0476$, respectively. That is, fewer than two cycles from the central high-intensity part of the incident laser pulse are transmitted. The transmission coefficient (consistent with the linear definition) is then $\mathcal{T} = a_{tr}/a_0 \sim 0.476$, which agrees fairly well with that estimated in Sec. I.

The envelopes of the incident and transmitted wave electric fields $|E|^{in}(t)$ and $|E|^{tr}(t)$ and that obtained from the Fresnel formula using the calculated refractive index N , as well as their spectral power densities (SPDs), are shown in Fig. 2. We see that the results from the simulation roughly agree with that from the Fresnel formula. Additional simulations (not shown) indicate that the discrepancy in the latter decreases (increases) for longer (shorter) magnetization pulses, and it can even vanish for very long pulses.

Figure 3(a) shows the envelope $|E|$ and the y projection E_y of the electric field of the two-cycle transmitted pulse at $x = 2.1\lambda_L$. Figure 3(b) shows that with respect to the input laser, the transmitted pulse is slightly frequency-shifted: first blue and then red, which can be attributed to the compression-relaxation sequence of the light pulse as it propagates through the target. This scenario can be more clearly seen in Fig. 3(c) for the corresponding SPD at different times. For example, the central frequencies at $t = 9.08T_L$, $t = 9.88T_L$, and $t = 10.88T_L$ are roughly $1.20\omega_L$, $1.09\omega_L$, and $0.88\omega_L$, respectively, accompanied by a slight broadening of the SPD profile. For specific

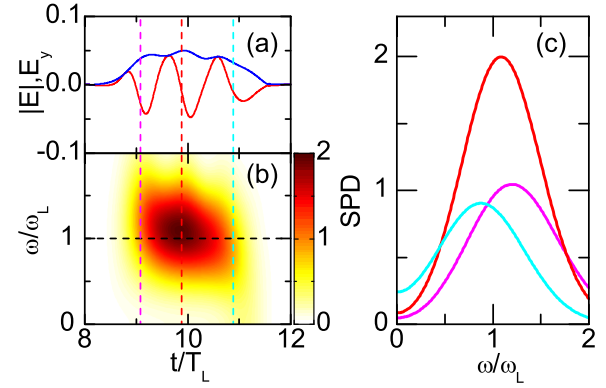


FIG. 3. (a) Evolution of the y component $E_y(t)$ (red solid curve) and the magnitude $|E(t)|$ (blue solid curve) of the electric field of the transmitted wave at $x = 2.1\lambda_L$, just outside the right edge of the target, and (b) the corresponding SPD (in arbitrary units, as obtained from short-time Fourier transform with a two-cycle Chebyshev window). (c) The corresponding SPD at $t = 9.08T_L$ (magenta), $t = 9.88T_L$ (red), and $t = 10.88T_L$ (cyan).

needs of the resulting short light pulse, one can optimize the input parameters. For example, since the transmitted pulse is not Fourier-, or bandwidth-, limited, further shortening through tailoring the timings, configurations, etc. of the laser and applied magnetic field should be possible. However, in order to avoid cyclotron resonance, the applied magnetic field should not be such that the electron cyclotron frequency is too near the laser frequency.

IV. DISCUSSION

To see more clearly the physical processes involved and what happens at longer times, in Fig. 4 we show the evolution of the total electric field in the y direction, the total magnetic field in the z direction, the electron density, and the y component of the plasma current density. One can see in panel (a) that about two cycles of the laser are transmitted. The magnetic field in (b) contains the fields of the periodic light wave as well as the quasistatic self-generated one, which can also be seen in Figs. 1(b) and 1(d) in the thin target at $x \sim 2$, especially after the laser pulse has ended at $t \gtrsim 18$. [Note that the applied magnetic field $B_0(t)$ that exists transiently between the two black dashed lines is in the x direction and therefore not color-coded.] The self-field also contains a small x component (not shown), which is, however, too weak to allow the rest of the RHCP laser pulse to penetrate the target since the laser light is now in the stopband between the electron cyclotron and the right-cutoff frequencies. (The other side of the stopband corresponds to the fast RHCP EMW branch that can propagate only in an underdense plasma [20].) As a result, most of the remaining laser light is reflected at the right target boundary, but a very small fraction is still transmitted. The latter is almost invisible in the vacuum on the right side of the target. However, since the peak wave magnetic field is of order ~ 0.20 , its periodic structure superimposed in the same ordered self-generated quasistationary magnetic field can be clearly observed inside the target. This partial self-induced transparency can be attributed to the ponderomotive force that

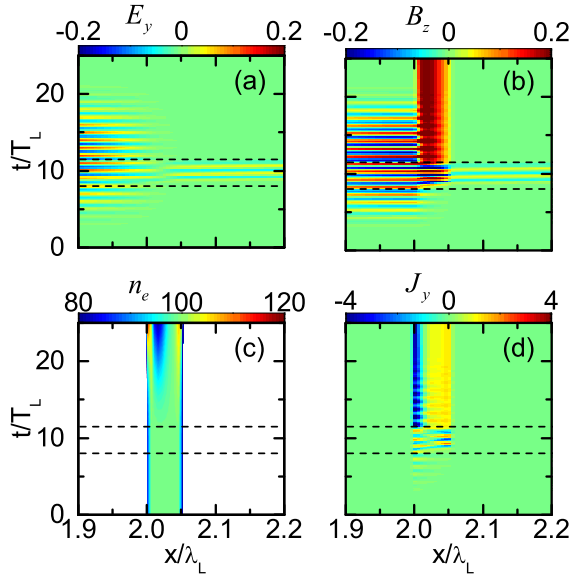


FIG. 4. (a) The y component $E_y(x,t)$ of the wave electric field. (b) The total magnetic field $B_z(x,t)$ in the z direction, consisting of the oscillating light wave and the static self-generated magnetic fields. (c) The electron density $n_e(x,t)$. (d) The y component $J_y(x,t)$ of the current density. The density depression appearing in (c) for $t \gtrsim 20$ is a result of the unstable bipolar, thus sheared, current distribution in (d).

effectively reduces the skin depth [2,3,29,30], as well as the thinness (not much larger than the skin depth $0.016\lambda_L$) of the target. For the same reason, very weak penetration (not observable in the figures) already took place as the front of the laser pulse impinges on the target, before the magnetic pulse is turned on. As expected, this weak self-transparency vanishes when the thickness of the target is increased.

It is worth noting that although the self-generated quasistatic magnetic field and the corresponding bipolar sheared current density found in Fig. 4(d) are created rapidly, they are relatively long-living, persisting even after the actions of both the driving magnetic and laser pulses have ended. Moreover, the plasma also remains quasineutral almost everywhere throughout the process. This behavior can be attributed to the fact that the present PIC simulation is collisionless, the initial target plasma is cold, the magnetic pulse is very short, and the incident laser pulse is not too intense, so that the plasma slab is not destroyed by the interaction. However, at still longer times ($t \gtrsim 20$), panel (c) shows that a depression in the plasma density starts to appear, since the oppositely propagating currents in (d) tend to repel each other. If

higher-dimensional effects are included, one can expect an appearance of shear-driven plasma instabilities that can destroy the self-magnetic field and the plasma [3,15,31,32]. However, such long-time behavior does not affect the process under consideration.

For simplicity, we have considered a spatially uniform magnetic field and a short laser pulse. In practice, the magnetic field is only needed inside the target, so that a highly space- and time-localized magnetic field (such as that produced in the interaction of ultraintense lasers with solid targets [16,17]) and longer laser pulses can also be used. Moreover, the interaction is of a very small time and space scale, so that it does not have to start from a steady state. For example, since magnetic fields of the required intensities are also generated by laser interaction with solid-density targets, it may be possible to design a setup that unifies the field generation and laser penetration processes by making use of the fast oscillating extremely large wave magnetic field of a second laser pulse.

V. CONCLUSION

In this paper, we have demonstrated with a simple model and PIC simulation that RHCP EMWs propagating in high-density plasma can be controlled with a magnetic pulse, and that the process can be used to generate an intense few-cycle laser pulse. It should be mentioned that the propagation and interaction of linear and nonlinear low-frequency RHCP electromagnetic waves in the radio- and microwave regimes have been widely studied for many decades in conjunction with wave propagation in space, ionospheric, and laboratory plasmas, where RHCP waves with $B_0 > 1$ correspond to the well-known whistler waves. The latter can propagate along the Earth's magnetic fields for long distances [20,33]. The phenomena considered here may also be relevant to modification of long-wavelength EM waves in the whistler wave regime in the laboratory and ionosphere modification experiments [34,35], EM wave-driven current drive and heating of magnetically confined fusion plasmas [20], as well as for interpreting phenomena observed in astrophysical environments, especially those involving magnetars, where dense plasmas, intense magnetic and radiation fields, as well as short time scales are prevalent [4,6,11].

ACKNOWLEDGMENTS

This work was supported by the National Natural Science Foundation of China (11475147, 11374262, 11304331, 11174303), the National Basic Research Program of China (2013CBA01504 and 2011CB808104), the State Key Laboratory of High Field Laser Physics at SIOM, and the Fundamental Research Funds for Central Universities.

- [1] W.-M. Wang, P. Gibbon, Z.-M. Sheng, and Y.-T. Li, *Phys. Rev. Lett.* **114**, 253901 (2015).
- [2] M. Y. Yu, P. K. Shukla, and K. H. Spatschek, *Phys. Rev. A* **18**, 1591 (1978).
- [3] X. H. Yang, W. Yu, H. Xu, M. Y. Yu, Z. Y. Ge, B. B. Xu, H. B. Zhuo, Y. Y. Ma, F. Q. Shao, and M. Borghesi, *Appl. Phys. Lett.* **106**, 224103 (2015).

- [4] R. F. Archibald, V. M. Kaspi, C.-Y. Ng, K. N. Gourgouliatos, D. Tsang, P. Scholz, A. P. Beardmore, N. Gehrels, and J. A. Kennea, *Nature (London)* **497**, 591 (2013).
- [5] R. Turolla, S. Zane, and A. L. Watts, *Rep. Prog. Phys.* **78**, 116901 (2015).
- [6] V. S. Beskin, A. Balogh, M. Falanga, and R. A. Treumann, *Space Sci. Rev.* **191**, 1 (2015).

- [7] E. L. Bichenkov, *J. Appl. Mech. Tech. Phys.* **41**, 792 (2000).
- [8] M. Jaime, R. Daou, S. A. Crooker, F. Weickert, A. Uchida, A. E. Feiguin, C. D. Batista, H. A. Dabkowska, and B. D. Gaulin, *Proc. Natl. Acad. Sci. USA* **109**, 12404 (2012).
- [9] L. Biermann, *Z. Naturforsch. A* **5**, 65 (1950).
- [10] E. S. Weibel, *Phys. Rev. Lett.* **2**, 83 (1959).
- [11] A. Gruzinov, *Astrophys. J.* **563**, L15 (2001).
- [12] M. Tatarakis, A. Gopal, I. Watts, F. N. Beg, A. E. Dangor, K. Krushelnick, U. Wagner, P. A. Norreys, E. L. Clark, M. Zepf, and R. G. Evans, *Phys. Plasmas* **9**, 2244 (2002).
- [13] V. S. Belyaev, V. P. Krainov, V. S. Lisitsa, and A. P. Matafonov, *Phys. Usp.* **51**, 793 (2008).
- [14] S. Fujioka, Z. Zhang, K. Ishihara, K. Shigemori, Y. Hironaka, T. Johzaki, A. Sunahara, N. Yamamoto, H. Nakashima, T. Watanabe, H. Shiraga, H. Nishimura, and H. Azechi, *Sci. Rep.* **3**, 1170 (2013).
- [15] Y. J. Gu, O. Klimo, D. Kumar, Y. Liu, S. K. Singh, T. Zh. Esirkepov, S. V. Bulanov, S. Weber, and G. Korn, *Phys. Rev. E* **93**, 013203 (2016).
- [16] U. Wagner, M. Tatarakis, A. Gopal, F. N. Beg, E. L. Clark, A. E. Dangor, R. G. Evans, M. G. Haines, S. P. D. Mangles, P. A. Norreys, M.-S. Wei, M. Zepf, and K. Krushelnick, *Phys. Rev. E* **70**, 026401 (2004).
- [17] D. J. Stark, T. Toncian, and A. V. Arefiev, *Phys. Rev. Lett.* **116**, 185003 (2016).
- [18] *ELI-Extreme Light Infrastructure Science and Technology with Ultra-Intense Lasers*, edited by G. A. Mourou, G. Korn, W. Sander, and J. L. Collier (THOSS, Berlin, 2011).
- [19] E. Hecht, *Optics*, 4th ed. (Addison-Wesley Longman, Boston, 2002).
- [20] F. F. Chen, *Introduction to Plasma Physics and Controlled Fusion*, 2nd ed. (Springer, New York, 2006).
- [21] T. Brabec and F. Krausz, *Rev. Mod. Phys.* **72**, 545 (2000).
- [22] M. Roth, T. E. Cowan, M. H. Key, S. P. Hatchett, C. Brown, W. Fountain, J. Johnson, D. M. Pennington, R. A. Snavely, S. C. Wilks, K. Yasuike, H. Ruhl, P. Pegoraro, S. V. Bulanov, E. M. Campbell, M. D. Perry, and H. Powell, *Phys. Rev. Lett.* **86**, 436 (2001).
- [23] M. Borghesi, A. Schiavi, D. H. Campbell, M. G. Haines, O. Willi, A. J. Mackinnon, P. Patel, M. Galimberti, and L. A. Gizzi, *Rev. Sci. Instrum.* **74**, 1688 (2003).
- [24] V. Malka, *Med. Phys.* **31**, 1587 (2004).
- [25] X. Q. Yan, C. Lin, Z. M. Sheng, Z. Y. Guo, B. C. Liu, Y. R. Lu, J. X. Fang, and J. E. Chen, *Phys. Rev. Lett.* **100**, 135003 (2008).
- [26] H.-C. Wu and J. Meyer-ter-Vehn, *Nat. Photon.* **6**, 304 (2012).
- [27] H. B. Zhuo, Z. L. Chen, Z. M. Sheng, M. Chen, T. Yabuuchi, M. Tampo, M. Y. Yu, X. H. Yang, C. T. Zhou, K. A. Tanaka, J. Zhang, and R. Kodama, *Phys. Rev. Lett.* **112**, 215003 (2014).
- [28] W. P. Leemans, A. J. Gonsalves, H.-S. Mao, K. Nakamura, C. Benedetti, C. B. Schroeder, Cs. Tóth, J. Daniels, D. E. Mittelberger, S. S. Bulanov, J.-L. Vay, C. G. R. Geddes, and E. Esarey, *Phys. Rev. Lett.* **113**, 245002 (2014).
- [29] Y. R. Shen, *The Principles of Nonlinear Optics* (Wiley-Interscience, New York, 1984).
- [30] E. Lefebvre and G. Bonnaud, *Phys. Rev. Lett.* **74**, 2002 (1995).
- [31] M. Faganello, F. Califano, and F. Pegoraro, *Phys. Rev. Lett.* **101**, 105001 (2008).
- [32] Q.-L. Dong, S.-J. Wang, Q.-M. Lu, C. Huang, D.-W. Yuan, X. Liu, X.-X. Lin, Y.-T. Li, H.-G. Wei, J.-Y. Zhong, J.-R. Shi, S.-E. Jiang, Y.-K. Ding, B.-B. Jiang, K. Du, X.-T. He, M. Y. Yu, C. S. Liu, S. Wang, Y.-J. Tang, J.-Q. Zhu, G. Zhao, Z.-M. Sheng, and J. Zhang, *Phys. Rev. Lett.* **108**, 215001 (2012).
- [33] P. H. Yoon, *Geophys. Res. Lett.* **38**, L12105 (2011).
- [34] P. Y. Cheung, D. F. DuBois, T. Fukuchi, K. Kawan, H. A. Rose, D. Russell, T. Tanikawa, and A. Y. Wong, *J. Geophys. Res.* **97**, 10575 (1992).
- [35] D. M. Wright, J. A. Davies, T. K. Yeoman, T. R. Robinson, and H. Shergill, *Ann. Geophys.* **24**, 543 (2006).